Photoelectron-angular-distribution parameters for rare-gas subshells

J. W. Cooper
Institute for Physical Science and Technology, University of Maryland, College Park, Maryland 20742
(Received 8 May 1992)

Formulas for the first-order corrections in α to the dipole form for the angular distribution for atomic photoionization are derived within a nonrelativistic central-potential model. The results are expressed in terms of two parameters γ and δ and simple expressions for the angular distribution for unpolarized, polarized, and partially polarized light are given. Calculations for a number of rare-gas subshells are presented and compared with previous calculations.

PACS number(s): 32.80.Fb, 32.80.Hd

I. INTRODUCTION

In a previous publication [1], it was pointed out that for incident photon energies of less than approximately 5 keV, the angular distribution of photoelectrons ejected from atoms for both polarized and unpolarized light could be adequately represented by two additional parameters in addition to the usual β parameter which, along with the total cross section for a particular process, completely describes the angular distribution within the dipole approximation. Similar conclusions were reached in recent nonrelativistic work on s and p subshells [2,3] and in a relativistic treatment [4].

The fact that corrections to dipole approximation can be expressed simply over a broad energy range has led to recent interest in experimental studies that would measure the "dipole-breakdown" parameters, since at present there are only two early experiments [5,6] which show deviations from dipole approximation at energies below 5 keV. It is the purpose of this paper to provide information that will be useful in planning such experiments. Specifically this includes (i) derivation of the relevant formulas within a nonrelativistic central-field model, (ii) calculation of parameters for typical experimental situations, and (iii) comparison of the calculations with previous work in order to access both their accuracy and the importance of relativistic effects. The outline of the paper is as follows. Section II contains the derivation of all of the appropriate formulas; Sec. III is devoted to calculations for the s, p, and d subshells of the rare gases; Sec. IV compares these calculations with previous calculations; and Sec. V gives suggestions for future theoretical and experimental work.

II. DIFFERENTIAL CROSS SECTION

The starting point is the expression for the differential cross section for photoionization of a single electron in atomic units by a photon of energy ω [7]:

$$\frac{d\sigma_{if}(\omega,\theta,\phi)}{d\Omega}=\frac{4\pi^2\alpha}{\omega}|D_{if}|^2 , \tag{1}$$

where the matrix element D_{if} between initial and final states is

$$D_{if}=\langle \psi_f^* e^{i\mathbf{k}\cdot\mathbf{r}}\boldsymbol{\epsilon}\cdot\mathbf{p}|\psi_i\rangle , \tag{2}$$

where $\mathbf{p}$ is the momentum operator, $\mathbf{k}$ is the photon momentum, and $\boldsymbol{\epsilon}$ is the polarization vector. Assuming that the photon direction is along the x axis and the polarization direction along the z axis as shown in Fig. 1, the matrix element may be written as

$$D_{if}=\left\langle \psi_f^* e^{ikx}\frac{\partial\psi_i}{\partial z}\right\rangle . \tag{3}$$

Expanding the exponential, to first order in $k=\alpha\omega$ the matrix element becomes

$$D_{if}\left\langle \psi_f^*\left|(1+ikx)\right|\frac{\partial\psi_i}{\partial z}\right\rangle . \tag{4}$$

As shown in Ref. [7], both terms in Eq. (4) can be converted to the "length" forms of the matrix element via the relations

$$\begin{aligned}\left\langle \psi_f^*\left|\frac{\partial}{\partial z}\right|\psi_i\right\rangle&=\omega\langle\psi_f^*|z|\psi_i\rangle ,\\ \left\langle \psi_f^*\left|ikx\frac{\partial}{\partial z}\right|\psi_i\right\rangle&=\frac{i\omega^2\alpha}{2}\langle\psi_f^*|xz|\psi^i\rangle-\frac{\omega\alpha}{2}\langle\psi_f^*|L_y|\psi_i\rangle ,\end{aligned} \tag{5}$$

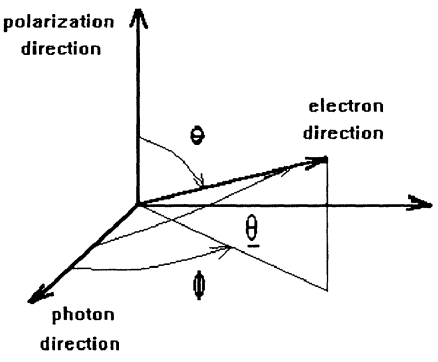

FIG. 1. Definition of the angles θ, ϕ and $\underline{\theta}$ used here relative to photon, electron, and polarization directions.

where L_y is the y component of the angular momentum operator $\mathbf{r}\times\mathbf{p}$. The three terms shown in Eq. (5) are simply the electric dipole, electric quadrupole, and magnetic dipole matrix elements used to describe spectroscopic transitions between discrete states. Although the expressions here are given only for a one-electron system, they also apply to many electron systems if the operators z, xz, and L_y are replaced by sums over all electrons, provided ψ_f and ψ_i are exact eigenstates of the nonrelativistic atomic Hamiltonian.

Equation (5) also shows that the electric quadrupole and magnetic dipole terms are proportional to α. Thus pure electric quadrupole or magnetic dipole transitions are generally smaller than dipole transitions by a factor of α^2, since they are proportional to the square of the matrix element for that type of transition, and may be neglected unless the electric dipole is vanishingly small. However, as will be shown, in calculating the angular distribution of photoelectrons, the dominant term is an interference term between the electric dipole and electric quadrupole term which will be proportional to α. Also note that the electric quadrupole term is proportional to ω^2, whereas the electric and magnetic dipole terms are proportional to ω, which means that the electric quadrupole term cannot be neglected at high photon energies. Although both the electric quadrupole and magnetic dipole terms are of the same order of α with respect to the electric dipole term, the magnetic dipole term is expected to be smaller at all energies for the following reason. The operator L_y operates only on the angular part of the wave function. In a single-electron approximation, this leads to the selection rules $\Delta l=0$ and $\Delta m=0,+1$ for the orbital and magnetic quantum numbers l and m, but the radial part of the wave function must change since energy is absorbed. In a central-field model, one-electron radial wave functions with the same value of l and different energies are orthogonal and the magnetic dipole term vanishes. It does not vanish if different potentials are used to describe initial and final one-electron states, as is the case when core relaxation of a many-electron atom is considered.

The parameter α is used rather than $Z\alpha$, since it is assumed that the Z dependence is contained in the radial wave functions corresponding to ψ_i and ψ_f, which are assumed to be obtained numerically by a nonrelativistic central-field calculation. Since it is well known that relativistic effects are important for large Z, some comments are in order on their relative magnitude. In a relativistic central-field model, the matrix element is modified in two ways, namely, (i) the operator $\mathbf{p}$ is replaced by a Pauli spin matrix and (ii) the initial- and final-state wave functions are replaced by two-component solutions of a Dirac central-field Hamiltonian. In addition, in evaluating the matrix element, the exponential factor in Eq. (2) is expanded in terms of electric and magnetic multiple moments. To first order in α this expansion leads to the same result as the simple expansion used here, and to this order, relativistic effects are due only to differences in the initial and final-state wave functions.

Neglecting the magnetic dipole term in Eq. (4) and simplifying notation, the matrix element may be written as

$$D_{if}=\omega\langle z\rangle_{if}+\frac{i\omega^2\alpha}{2}\langle xz\rangle_{if}\ . \tag{6}$$

If Eq. (1) is taken to represent all N_{n1} electrons in a given closed atomic subshell, the cross section for that subshell, using the matrix element of Eq. (6), can be written as

$$\frac{d\sigma_{nl}(\omega,\theta,\phi)}{d\Omega}=4\pi^2\alpha N_{nl}\omega[\langle z\rangle\langle z\rangle^*+i\alpha\omega/2(\langle xz\rangle\langle z\rangle^*-\langle z\rangle\langle xz\rangle^*)]+O(\alpha^2)\ , \tag{7}$$

where each single-electron matrix element $\langle xz\rangle$ and $\langle z\rangle$ is to be evaluated between initial and final states.

Choosing the outgoing electron's direction as the axis of quantization, the initial- and final-state wave functions for an electron in the (nl)th subshell may be represented as

$$\psi_i=P_{nl}(r)Y_{lm}(\theta',\phi') \tag{8}$$

and

$$\psi_f=\sum_{l'}[4\pi(2l'+1)]^{1/2}(i)^{l'}e^{-i\delta_{l'}}P_{\omega l'}(r)Y_{l'0}(\theta',\phi')\ . \tag{9}$$

The factors z and xz appearing in the matrix elements of Eq. (7) are represented in terms of r and the angles θ and ϕ shown in Fig. 1 as

$$\begin{aligned} z&=r\cos\theta=\sqrt{4\pi/3}rY_{1,0}(\theta,\phi)\\ xz&=r^2\sin\theta\cos\theta\cos\phi\\ &=2\sqrt{2\pi/3}Y_{1,0}(\theta,\phi)[Y_{1,-1}(\theta,\phi)+Y^*_{1,1}(\theta,\phi)]\\ &=\sqrt{2\pi/15}r^2[Y_{2,-1}(\theta,\phi)-Y_{2,1}(\theta,\phi)]\ . \end{aligned} \tag{10}$$

The mth component of the matrix elements for z and xz can then be written as

$$\langle z\rangle_m=(4\pi^3/3)^{1/2}\sum_{l'}(2l'+1)^{1/2}(i)^{-l'}e^{i\delta_{l'}}\langle P_{nl}|r|P_{\omega l'}\rangle \times\langle Y_{lm}(\theta',\phi')Y_{10}(\theta,\phi)Y^*_{l'0}(\theta',\phi')\rangle\ , \tag{11}$$

and

$$\langle xz\rangle_m[32\pi^3/(15)]^{1/2}\sum_{l''}(2l''+1)^{1/2}i^{-l''}e^{i\delta_{l''}}\langle P_{nl}|r^2|P_{\omega l''}\rangle x\langle Y_{lm}(\theta',\phi')[Y_{2-1}(\theta,\phi)-Y_{21}(\theta,\phi)]Y_{l''0}(\theta',\phi')\rangle\ , \tag{12}$$

where integration over the variables r, θ', and ϕ' is implied. Explicit expressions for the cross section are obtained by inserting Eqs. (11) and (12) in Eq. (7) and carrying out the integrations and summations over m, l', and l''. For the first term of Eq. (7), this procedure leads to the usual dipole form for the differential cross section [8]:

$$\frac{d\sigma_{nl}}{d\Omega}=\frac{\sigma_{nl}}{4\pi}[1+\beta P_2(\cos\theta)] , \tag{13}$$

where the total cross section for the (nl)th subshell is given in terms of the radial dipole matrix elements $R_{\omega l\pm1}$ and phase shifts $\delta_{l\pm1}$:

$$\sigma_{nl}=\frac{4\pi^2\alpha}{3(2l+1)}N_{nl}\omega[lR^2_{\omega,l-1}+(l+1)R^2_{\omega,l+1}] , \tag{14}$$

and the β parameter is

$$\beta=\frac{l(l-1)R^2_{\omega,l-1}+(l+1)(l+2)R^2_{\omega,l+1}-6l(l+1)R_{\omega,l-1}R_{\omega l+1}\cos(\delta_{l+1}-\delta_{l-1})}{(2l+1)[lR^2_{\omega,l-1}+(l+1)R^2_{\omega,l+1}]} \tag{15}$$

In order to obtain the angular dependence of the cross section from Eq. (7), the imaginary part of the sum of the product of the matrix elements $\langle z\rangle_m$ and $\langle xz\rangle_m$ must be evaluated. This can be done by expressing the factors in Eq. (11) and (12) that depend on θ and ϕ in terms of rotation matrices as was done in previous work on molecular systems [9]. Writing

$$Y_{10}(\theta,\phi)=\sum_{\bar m}Y_{1\bar m}(\theta',\phi')D^{(1)}_{\bar m0}(\alpha,\beta,\gamma) , \tag{16}$$

where $D^{(k)}_{ij}(\alpha,\beta,\gamma)$ is a rotation matrix [10], the dipole matrix element then becomes

$$\langle z\rangle^*_m=(4\pi^3/3)^{1/2}\sum_{\bar m l'}(2l'+1)^{1/2}R_{\omega,l'}i^{l'}e^{-i\delta_{l'}}\langle Y^*_{lm}Y_{1\bar m}Y_{l'0}\rangle D^{(1)}_{\bar m0}(\alpha,\beta,\gamma) . \tag{17}$$

Similarly, by expressing $Y_{2-1}(\theta,\phi)$ and $Y_{21}(\theta,\phi)$ in terms of rotation matrices, Eq. (12) may be written as

$$\langle xz\rangle_m=(32\pi^3/15)^{1/2}\sum_{l'',M}\langle P_{nl}r^2P_{\omega l''}\rangle(2l''+1)^{1/2}i^{-l''}e^{i\delta_{l''}}\langle Y_{lM}Y_{2M}Y_{l''0}\rangle[D^{(2)}_{M1}(\alpha,\beta,\gamma)-D^{(2)}_{M-1}(\alpha,\beta,\gamma)] . \tag{18}$$

Taking the product of Eqs. (17) and (18), recoupling the rotation matrices, and evaluating the angular integrals yields

$$\begin{aligned}\langle z\rangle^*_m\langle xz\rangle_m=16\frac{\pi^2}{\sqrt{6}}(-1)^m\sum_{(l',l'',L)}&\langle R_{\omega,l'}\rangle\langle P_{nl}r^2P_{\omega l''}\rangle i^{l'-l''}e^{-i(\delta_{l'}-\delta_{l''})}(2l+1)(2L+1)(2l'+1)(2l''+1)\\&\times\begin{bmatrix}l&1&l'\\0&0&0\end{bmatrix}\begin{bmatrix}1&l&l'\\m&-m&0\end{bmatrix}\begin{bmatrix}l&2&l''\\0&0&0\end{bmatrix}\begin{bmatrix}l&2&l''\\m&-m&0\end{bmatrix}\begin{bmatrix}1&2&L\\m&-m&0\end{bmatrix}\\&\times\begin{bmatrix}1&2&L\\0&-1&1\end{bmatrix}[D^{(L)*}_{0,-1}(\alpha,\beta,\gamma)+D^{(L)}_{0,-1}(\alpha,\beta,\gamma)] .\end{aligned} \tag{19}$$

The sum of rotation matrices in Eq. (19) is real and may be expressed in terms of spherical harmonics as

$$\begin{aligned}&D^{(L)}_{0,-1}(\alpha,\beta,\gamma)+D^{(L)*}_{0,-1}(\alpha,\beta,\gamma)\\&\quad=+\left[\frac{4\pi}{2L+1}\right]^{1/2}[Y_{L,-1}(\beta,\alpha)+Y^*_{L,-1}(\beta,\alpha)] .\end{aligned} \tag{20}$$

The rotation angles β and α are simply the angles θ and ϕ as shown in Fig. 1.

An explicit form of the angular distribution produced by the second term in Eq. (7) is given in Appendix A. The following are the important features.

(i) The usual dipole and quadrupole selection rules $l'=l\pm1$ and $l''=l,l\pm2$ are implied by the $3j$ coefficients in Eq. (19).

(ii) The added term will be proportional to $\cos\phi$. The $L=1$ term introduces a $\sin\theta$ dependence and $L=3$ term both a $\sin\theta$ and a $\sin\theta\cos^2\theta$ dependence.

(iii) Only $L=1$ and $L=3$ terms are permitted by the selection rules. This is obvious since dipole absorption corresponds to transfer of one unit of angular momentum and quadrupole absorption to two or zero units and agrees with an analysis based on more general considerations [11].

(iv) The summations over m to be carried out in evaluating the cross section only extend over the value $0,\pm1$.

As indicated in Ref. [1], the added term in the angular distribution can be expressed in terms of two additional parameters γ and δ and the cross section for linearly polarized light written as

$$\frac{d\sigma_{nl}}{d\Omega}=\frac{\sigma_{nl}}{4\pi}[1+\beta P_2(\cos\theta)+(\delta+\gamma\cos^2\theta)\sin\theta\cos\phi] . \tag{21}$$

Previous work on angular distributions [12,13] has concentrated on expressing the angular distribution for unpolarized light in terms of an expansion in Legendre polynomials in the angle $\underline{\theta}$ with respect to the incident photon direction as

$$\frac{d\sigma_{nl}}{d\Omega}=\frac{\sigma_{nl}}{4\pi}\sum_n B_n P_n(\cos\underline{\theta}) , \tag{22}$$

and relativistic central-field calculations have been carried out to determine the B_n parameters. In Ref. [4], the angular distribution for polarized light is shown to be to good approximation expressed in terms of the three parameters B_1, B_2, and B_3 and expressions for these parameters to first order in $k=\omega\alpha$ have been given previously for the nonrelativistic case [14]. More recently [2,3] calculations for K and L subshells have been performed in a nonrelativistic framework. To first order in α all of these formulations lead to the same form for the angular distributions for both polarized and unpolarized light. The relationships between the parameters used by various authors is given in Table I. In terms of the parameters β, γ, and δ the angular distribution for unpolarized light is

$$\frac{d\sigma_{nl}}{d\Omega}=\frac{\sigma_{nl}}{4\pi}\left[1-\beta/2P_2(\cos\underline{\theta})+\left[\frac{\gamma}{2}\sin^2\underline{\theta}+\delta\right]\cos\underline{\theta}\right] . \tag{23}$$

Equation (21) gives the cross section for light polarized in the z direction. If the z direction is taken as the principal axis of polarization and the fraction of light polarized in the z direction is represented by P [15], the cross section for partially polarized light is

$$\frac{d\sigma_{nl}}{d\Omega}=\frac{\sigma_{nl}}{4\pi}\left[1+\frac{\beta}{4}+\frac{3}{4}P\beta\cos2\theta\right] + \left\{\gamma\left[P\cos^2\theta-\frac{(P-1)}{2}(1-\sin^2\theta\cos^2\phi)\right] +\delta\right\}\sin\theta\cos\phi . \tag{24}$$

As shown in Appendix B, for s subshells only $m=0$ magnetic quantum numbers contribute. As a result, the δ term in the angular distribution vanishes or $B_1=B_3$, as has been shown in previous work [2,3,14].

TABLE I. Relationships between the parameters β, a, and b used in Ref. [3], the parameters B_1, B_2, and B_3 of Ref. [4], and the parameters β, γ, and η of Ref. [14] with the parameters β, γ, and δ used in this paper.

Parameter	Ref. [3]	Ref. [4]	Ref. [14]
β	β	$-B_2/2$	β
γ	$3/2b$	$-5B_3$	$-5\omega\alpha\eta$
δ	$a-1/2b$	B_1+B_3	$\omega(\gamma+\eta)$

III. COMPUTATIONS OF THE ANGULAR-DISTRIBUTION PARAMETERS

Experiments that provide information on the angular distributions of photoelectrons from specific subshells will most likely be done on rare-gas targets using synchrotron light sources at photon energies between 15 eV and 10 keV. In order to identify those regions where departures of the angular distribution from the usual dipole result, calculations have been made of the parameters γ, β, and δ for electron energies between 100 eV and 5 keV and are shown in Tables II–IX for a number of rare-gas subshells using a central-field model based on the Herman-Skillman potential [15]. The calculations have been limited to this energy range since at electron energies near threshold, the central-field model will be inaccurate due to interchannel interactions, and at higher energies the cross sections are so low that it is unlikely that angular distributions can be measured.

The method of calculation is similar to earlier work [16]. In order to calculate the additional parameters γ and δ using the equations given in Appendix A, the only additional calculations that are necessary are those of the

TABLE II. Cross sections and δ parameters for helium and neon s subshells. Values of γ from Refs. [2] and [3] are shown in parentheses. The cross sections listed are in units of kb; i.e., 10^{-21} cm^2.

Energy (eV)		Cross section	γ
Electron	Photon	(kb)	
		Helium 1s	
100	123	202.90	0.18
200	223	41.19	0.28
500	523	3.24	0.51
1000	1023	0.37	0.74
2000	2023	0.04	0.92
3000	3023	0.01	1.79
4000	4023	0.00	1.32
5000	5023	0.00	1.93
		Neon 2s	
100	143	401.30	−0.021 (−0.021)
200	243	186.48	−0.020 (−0.020)
500	543	41.27	0.162 (0.160)
1000	1043	9.62	0.424 (0.420)
2000	2043	1.81	0.797 (0.789)
3000	3043	0.64	1.05 (1.06)
4000	4043	0.32	1.21
5000	5043	0.18	1.53 (1.60)
		Neon 1s	
100	957	261.31	0.021 (0.021)
200	1057	201.59	0.125 (0.124)
500	1357	108.59	0.343
1000	1857	47.89	0.584 (0.582)
2000	2857	14.66	0.921 (0.918)
3000	3857	6.23	1.176
4000	4857	3.18	1.390
5000	5857	1.83	1.579

$l, l\pm2$ radial wave functions, and the evaluation of their phase shifts and quadruple matrix elements with the initial nl ground-state orbitals.

In a central-potential model, calculations performed in the "length" and "velocity" formulations are identical. Comparison of the results obtained using alternative forms for the radial dipole matrix elements thus serves as a check on the numerical accuracy of the calculations but gives no indication how good the approximation is. Alternative forms have been used for the quadrupole radial matrix elements as a check on the calculations and the derivation of the "velocity" form is given in Appendix C. All parameters are usually given to two decimal places, which corresponds to the approximate numerical accuracy of the calculations based on agreement between the length and velocity forms of the radial matrix elements. Electron energies are energies above threshold. The theoretical binding energies of each subshell [15] have been used to obtain the relevant photon energies.

For s subshells as shown in Appendix B, the δ parameter vanishes and in our approximation $\beta=2$. In Tables II–V subshell cross sections and γ parameters are listed for all s subshells of the rare gases with the exception of the $2s$ subshell of xenon and the $1s$ subshells of krypton and xenon, which are not included since the binding energies of these subshells are too large for the approximations used here to be valid. Comparisons are also given with the work of Refs. [2] and [3].

For the $1s$ and $2s$ subshells, the calculations show good agreement with the results of Refs. [2] and [3] and show the same energy dependence. The argon $1s$ and neon $2s$ γ parameters are negative at low energies due to the difference in dipole p and quadrupole d wave phase shifts and the γ parameters increase at higher energies. The argon and krypton $2s$ γ parameters are large at low energies and go through a negative minimum at higher energies.

The γ parameters of the outer s subshells of argon and krypton have the same energy dependence as the $2s$ subshells and are approximately the same at equal electron energies above 500 eV. This is not surprising since in a central-field approximation the phase shifts are the same for all ns subshells, and at higher energies the ratio of the dipole and quadrupole matrix elements is determined principally by the normalization of the continuum wave functions as discussed in Ref. [2].

TABLE III. Argon s subshell cross sections and γ parameters.

Energy (eV)		Cross section (kb)	γ
Electron	Photon		
	Argon $1s$		
100	3264	74.47	−0.16
200	3364	69.96	−0.04
500	3664	56.41	0.20
1000	4164	40.62	0.45
2000	5164	23.19	0.80
3000	6164	14.45	1.06
4000	7164	9.59	1.28
5000	8164	6.67	1.47
	Argon $2s$		
100	411	245.09	0.23
200	511	183.53	0.04
500	811	86.49	−0.04
1000	1311	34.72	0.12
2000	2311	10.33	0.46
3000	3311	4.49	0.74
4000	4311	2.37	0.98
5000	5311	1.40	1.19
	Argon $3s$		
100	129	223.48	0.14
200	229	98.53	0.03
500	529	23.60	−0.03
1000	1029	6.60	0.10
2000	2029	1.59	0.42
3000	3029	0.65	0.68
4000	4029	0.34	1.00
5000	5029	0.21	1.04

TABLE IV. Cross sections and γ parameters for krypton s subshells.

Energy (eV)		Cross section (kb)	δ
Electron	Photon		
	Krypton $2s$		
100	1944	68.79	0.83 (0.85)
200	2044	63.85	0.59 (0.64)
500	2344	51.06	0.19 (0.22)
1000	2844	36.65	−0.03 (−.02)
2000	3844	21.37	−0.03 (−.05)
3000	4844	13.89	0.11 (0.08)
4000	5844	10.56	0.30
5000	6844	7.74	0.48 (0.43)
	Krypton $3s$		
100	368	176.57	0.41
200	468	134.07	0.35
500	768	66.96	0.14
1000	1268	29.53	−0.03
2000	2268	10.33	−0.06
3000	3268	5.04	0.07
4000	4268	2.91	0.24
5000	5268	1.87	0.41
	Krypton $4s$		
100	126	138.48	0.20
200	226	64.00	0.23
500	526	17.43	0.12
1000	1026	5.64	−0.03
2000	2026	1.62	−0.05
3000	3026	0.73	0.08
4000	4026	0.40	0.22
5000	5026	0.26	0.37

The γ parameters for the 3*s*, 4*s*, and 5*s* subshells of xenon show a different behavior. γ is large at low energies and goes through a negative minimum at approximately 3 keV for all three subshells.

Parameters for the *p* subshells of neon, argon, krypton, and xenon are shown in Tables VI–VIII. Here all three angular distribution parameters are listed in addition to the subshell cross section and comparisons are made with the data of Ref. [3] for argon and krypton 2*p* subshells. The agreement with Ref. [3] is not as good as for the *ns* subshells, but all parameters have the same energy dependence.

The energy dependence of all parameters is the same for the *p* subshells of neon and argon, β decreasing with increasing energy, and the other two parameters increasing. The β parameters are approximately the same for the 2*p* and 3*p* subshells of argon at higher energies, but not for γ and δ. For the krypton and xenon subshells the key results are that the δ parameter is small over the entire energy range and the β and γ parameters show the same energy dependence and are approximately the same at higher energies for the krypton 2*p* and 3*p* and for the xenon 3*p* and 4*p* subshells.

Results for the krypton 3*d* subshell and the 3*d* and 4*d* subshells of xenon are shown in Table IX. For the 3*d* subshells the β parameter goes through a maximum and the γ and δ parameters increase with energy. The β parameter for the 4*d* subshell of xenon changes sign between electron energies of 100 and 200 eV. As is the case with other subshells, the parameters for both the 3*d* and 4*d* subshells of xenon are approximately equal at the higher energies.

TABLE V. Cross sections and γ parameters for xenon *s* subshells.

Energy (eV)		Cross section (kb)	δ
Electron	Photon		
	Xenon 3*s*		
100	1147	80.49	0.77
200	1247	71.42	0.64
500	1547	51.76	0.39
1000	2047	32.98	0.15
2000	3047	16.51	−0.06
3000	4047	9.79	−0.11
4000	5047	6.41	−0.08
5000	6047	4.49	−0.00
	Xenon 4*s*		
100	293	167.46	0.35
200	393	118.02	0.36
500	693	52.21	0.28
1000	1193	21.34	0.12
2000	2193	7.16	−0.05
3000	3193	3.54	−0.10
4000	4193	2.09	−0.08
5000	5193	1.37	−0.01
	Xenon 4*s*		
100	122	111.58	0.20
200	222	49.57	0.26
500	522	13.50	0.24
1000	1022	4.35	0.12
2000	2022	1.25	−0.05
3000	3022	0.58	−0.08
4000	4022	0.34	−0.08
5000	5022	0.22	−0.00

IV. COMPARISON WITH OTHER CALCULATIONS

Comparisons have already been made in Tables II, IV, VI, and VII with the results of Refs. [2] and [3]. In order to provide an indication of the size of relativistic effects, comparisons of the nonrelativistic calculations have been made with the results of Ref. [4] for the 3*d* and 4*d* subshells of barium and for all subshells of neon. The results are shown in Table X. Several things are to be noted from this comparison. First, the parameters are almost exactly the same for the spin-orbit-split components of each subshell. Second, the nonrelativistic cross sections and angular distribution parameters agree reasonably well with the relativistic calculations. The comparison indicates that in this energy range the nonrelativistic calculations may be used to provide an indication of the energy dependence of the parameters. Dirac-Fock calculations of β parameters and cross sections for photon energies for all elements in the photon energy range from 100 to 4500 eV have been performed at selected energies [17]. Comparisons of these data with nonrelativistic calculations generally show good agreement with nonrelativistic results. An example of the typical agreement is shown in Table XI. It should also be mentioned that the β parameters and cross sections for many of the rare-gas subshells listed here have been reported previously at the lower energies and compared with Hartree-Fock calculations [18].

V. SUGGESTIONS FOR FUTURE WORK

No comparisons with experimental data have been given here, principally because the only two experiments which show deviations from dipole approximation [5,6] were not performed with enough accuracy to extract additional parameters, although a direct comparison of the data with a relativistic calculation has been made [19]. The aim has been to provide data and simple formulas useful for planning future experiments. In this regard, a number of comments can be made.

First, in a sense, it is easier to observe dipole breakdown with unpolarized sources than with polarized light, since only one angle is involved and, in fact, the earlier measurements used unpolarized sources. In those measurements, made on neon 2*p* and krypton 3*s*, 3*p*, and 3*d* subshells, the angular distributions all peak at $\theta = 90°$ and slight shifts of the peak from the 90° due to the added terms are easily detected. Second, as has been pointed out previously [2–4], corrections to dipole approximation are by no means negligible at lower energies. However, as was pointed out previously [1], provided electrons are detected in the plane of polarization; i.e., perpendicular to the photon direction, the correction terms vanish. In order to observe dipole breakdown, the angu-

TABLE VI. Cross sections and β, γ, and δ parameters for argon $2p$ and $3p$ and the neon $2p$ subshells. Data from Ref. [3] is shown in parentheses.

Energy (eV)		Cross section (kb)	γ	β	δ
Electron	Photon				
			Argon $2p$		
100	348	2047.44	0.01 (−0.02)	1.26 (1.26)	0.01 (0.01)
200	448	1164.39	0.07	1.43	0.01
500	748	305.07	0.24 (0.27)	1.46 (1.46)	0.03 (0.02)
1000	1248	70.03	0.42 (0.48)	1.32 (1.32)	0.05 (0.03)
2000	2248	11.24	0.61 (0.71)	1.07 (1.04)	0.09 (0.07)
3000	3248	3.35	0.71	0.90	0.13
4000	4248	1.35	0.77	0.77	0.17
5000	5248	0.64	0.81 (0.96)	0.68 (0.55)	0.21 (0.17)
			Argon $3p$		
100	114	896.16	0.00	1.44	−0.01
200	214	360.22	0.02	1.62	0.00
500	514	55.54	0.19	1.55	0.02
1000	1014	9.80	0.39	1.36	0.04
2000	2014	1.35	0.46	1.07	0.07
3000	3014	0.40	0.73	0.89	0.14
4000	4014	0.14	1.19	0.72	0.26
5000	5014	0.08	1.36	0.69	0.35
			Neon $2p$		
100	120	2322.74	0.08	1.48	0.01
200	220	530.87	0.15	1.46	0.02
500	520	44.37	0.29	1.19	0.04
1000	1020	5.03	0.40	0.87	0.08
2000	2020	0.47	0.49	0.55	0.15
3000	3020	0.11	0.44	0.43	0.17
4000	4020	0.04	0.35	0.43	0.15
5000	5020	0.01	0.64	0.20	0.36

TABLE VII. Cross sections and β, γ, and δ parameters for krypton $2p$ and $3p$ subshells. Data from Ref. [3] is shown in parentheses.

Energy (eV)		Cross section (kb)	γ	β	δ
Electron	Photon				
			Krypton $2p$		
100	1777	476.12	−0.07 (−0.18)	0.99 (0.96)	−0.02 (0.00)
200	1877	420.11	−0.10	1.18	−0.01
500	2177	284.64	−0.01 (−0.06)	1.37 (1.38)	0.01 (0.03)
1000	2677	163.12	0.20 (0.19)	1.44 (1.46)	0.03 (0.03)
2000	3677	67.57	0.51 (0.57)	1.42 (1.43)	0.05 (0.03)
3000	4677	33.91	0.73 (0.83)	1.35 (1.35)	0.08 (0.06)
4000	5677	21.19	0.87	1.28	0.10
5000	6677	12.96	1.04 (1.17)	1.22 (1.57)	0.13 (0.09)
			Krypton $3p$		
100	307	710.72	0.24	0.88	0.04
200	407	607.89	0.24	1.31	0.00
500	707	302.85	0.01	1.58	−0.01
1000	1207	115.03	0.04	1.61	0.01
2000	2207	30.54	0.32	1.51	0.03
3000	3207	12.17	0.55	1.41	0.05
4000	4207	6.57	0.71	1.32	0.07
5000	5207	3.66	0.89	1.24	0.10

TABLE VIII. Cross sections and β, γ, and δ parameters for xenon $3p$ and $4p$ subshells.

Energy (eV)		Cross section (kb)	γ	β	δ
Electron	Photon				
		Xenon $3p$			
100	1024	382.75	0.37	0.92	0.10
200	1124	342.27	0.44	1.20	0.05
500	1424	243.06	0.21	1.48	0.00
1000	1924	145.85	0.01	1.59	0.00
2000	2924	63.77	0.06	1.60	0.01
3000	3924	33.34	0.24	1.56	0.02
4000	4924	19.52	0.43	1.51	0.03
5000	5924	12.35	0.61	1.47	0.05
		Xenon $4p$			
100	249	470.94	0.05	0.63	0.02
200	349	381.60	0.27	1.20	0.01
500	649	1.88.59	0.23	1.60	−0.01
1000	1149	77.43	0.02	1.70	−0.01
2000	2149	23.94	0.03	1.67	0.00
3000	3149	10.71	0.19	1.61	0.01
4000	4149	5.73	0.37	1.55	0.03
5000	5149	3.42	0.54	1.49	0.04

TABLE IX. Cross sections and β, γ, and δ parameters for krypton $3d$ and xenon $3d$ and $4d$ subshells.

Energy (eV)		Cross section (kb)	γ	β	δ
Electron	Photon				
		Krypton $3d$			
100	197	5738.10	0.00	0.48	0.01
200	297	3542.55	0.02	0.90	0.02
500	597	728.06	0.14	1.19	0.04
1000	1097	126.17	0.32	1.18	0.07
2000	2097	15.14	0.56	1.00	0.13
3000	3097	3.82	0.70	0.86	0.19
4000	4097	1.42	0.79	0.75	0.24
5000	5097	0.67	0.84	0.68	0.29
		Xenon $3d$			
100	793	2411.22	−0.02	0.45	−0.01
200	893	1829.46	−0.04	0.68	−0.01
500	1193	910.76	−0.01	1.04	0.02
1000	1693	351.62	0.16	1.19	0.05
2000	2693	87.43	0.46	1.18	0.09
3000	3693	31.59	0.67	1.10	0.13
4000	4693	14.05	0.82	1.02	0.17
5000	5693	7.16	0.93	0.95	0.21
		Xenon $4d$			
100	172	472.25	−0.12	−0.83	0.10
200	272	919.09	0.17	0.42	0.00
500	572	482.78	0.00	1.18	0.00
1000	1072	141.91	0.08	1.33	0.02
2000	2072	27.12	0.37	1.25	0.06
3000	3072	8.92	0.58	1.14	0.10
4000	4072	3.96	0.76	1.04	0.15
5000	5072	2.13	0.82	0.96	0.18

TABLE X. Relativistic (Ref. [4]) and nonrelativistic (this paper) cross sections (in kb) and angular-distribution parameters for neon 1*s*, 2*s*, and 2*p* subshells and barium 3*d* and 4*d* subshells at 3-keV photon energy. The sum of the spin-orbit-split components of each subshell should be compared with the nonrelativistic results.

Subshell	σ_R	σ_{NR}	γ_R	γ_{NR}	β_R	β_{NR}	δ_R	δ_{NR}
Ne 1*s*	12.8	13.0	0.95	0.96	1.96	2.0	0.002	0.00
Ne 2*s*	0.64	0.67	1.04	1.04	1.95	2.0	0.002	0.00
Ne $2p_{1/2}$	0.039	0.114	0.61	0.41	0.35	0.45	0.16	0.16
N2 $2p_{3/2}$	0.076		0.61		0.35		0.16	
sum	0.115							
Ba $3d_{3/2}$	31.8	76.7	0.52	0.49	1.20	1.17	0.087	0.095
Ba $3d_{4/2}$	44.9		0.54		1.17		0.087	
sum	76.7							
Ba $4d_{3/2}$	5.0	12.0	0.61	0.54	1.22	1.17	0.076	0.094
Ba $4d_{5/2}$	7.0		0.62		1.17		0.079	
sum	12.0							

lar distribution must be measured outside of the plane of polarization.

While in principle, dipole breakdown could be observed in any of the rare-gas subshells, the 4*d* subshell of xenon seems to be the most interesting case. The β parameter for this subshell has been measured [20] and goes through a negative minimum, and is zero at approximately 180- and 240-eV photon energy. At these energies the angular distribution in the dipole approximation would be isotropic and any anisotropy observed must be due to dipole breakdown.

On the theoretical side, while the calculations reported here provide a first-order estimate of the effects of dipole breakdown, further work is needed to extend the calculation of the angular distribution parameters to cases where intershell coupling is expected to modify the single-electron results.

TABLE XI. A comparison of relativistic (Ref. [17]) and nonrelativistic (this paper) cross sections (in kb) and β parameters for the xenon 4*d* subshell at selected energies. The listed relativistic cross sections are the sum of the spin-orbit-split $\frac{3}{2}$ and $\frac{5}{2}$ cross sections. β parameters are shown only for the $3d_{3/2}$ component and a 2.5-eV adjustment was made in the 4*d* binding energy in order to compare at equal electron energies.

Photon energy (eV)	σ_R	σ_{NR}	β_R	β_{NR}
132.3	773	845	1.83	1.83
151.1	399	405	0.34	0.16
184.0	531	546	−0.83	−0.72
676.5	354	365	1.07	1.25
1041.0	148	152	1.31	1.33
1486.6	64	65	1.35	1.31
4509.0	2.6	2.0	1.10	1.01

ACKNOWLEDGMENT

This work was partially supported by the National Science Foundation under Grant No. PHY-91-07337.

APPENDIX A

In order to obtain explicit expressions for the parameters γ and δ in terms of phase shifts and dipole and quadrupole radial matrix elements, summations over m, l', l'', and L must be performed over the product given in Eq. (19) of the dipole and quadrupole matrix elements, where the selection rules limit the values of l' and l'' to $l'=l\pm1$, $l''=l,l\pm2$. Defining the quadrupole radial matrix element

$$Q_{\omega l''}=\langle R_{nl}r^2R_{\omega l''}\rangle \ , \tag{A1}$$

the γ and δ parameters may be expressed in terms of the radial dipole matrix elements $R_{\omega,l\pm1}$ and the quadrupole radial matrix elements as

$$\gamma=\frac{3\omega\alpha}{2[lR_{l-1}^2+(l+1)R_{l+1}^2]}\times\sum_{l',l''}A_{l',l''}R_{\omega,l'}Q_{\omega,l''}\cos(\delta_{l''}-\delta_{l'}) \ ,$$

$$\delta=\frac{3\omega\alpha}{2[lR_{l-1}^2+(l+1)R_{l+1}^2]}\times\sum_{l',l''}B_{l',l''}R_{\omega,l'}Q_{\omega,l''}\cos(\delta_l''-\delta_1') \ . \tag{A2}$$

The coefficients in Eq. (A2) are given in Table XII. Note that for *s* subshells all terms vanish except $l'=l+1$ and $l''=l+2$ and that for *p* subshells there is no term for $l''=l-2$. The equations agree with the previous work of Refs. [2,3,14]. If individual contributions in terms of the parameters B_1 and B_3 of Eq. (22) are required, they may be obtained using the relations $B_1=\delta-\gamma/5$:

TABLE XII. The coefficients $A_{l',l''}$ and $B_{l',l''}$ of equation (A2).

l'	l''	$A_{l',l''}$	$B_{l',l''}$
$l-1$	$l-2$	$\frac{-(l(l-1)(1-2)}{(2l+1)(2l-1)}$	$\frac{-l(l+1)(l-1)}{(2l+1)(2l-1)}$
$l-1$	l	$\frac{2l(l-1)(l+1)}{(2l+3)(2l-1)}$	$\frac{l(l+1)}{(2l+3)(2l-1)}$
$l-1$	$l+2$	$\frac{-5l(l+2)(l+1)}{(2l+3)(2l+1)}$	$\frac{1(l+1)(l+2)}{(2l+3)(2l+1)}$
$l+1$	$l-2$	$\frac{-5l(1+1)(1-1)}{(2l+1)(2l-1)}$	$\frac{-l(1-1)(1+1)}{(2l+1)(2l-1)}$
$l+1$	l	$\frac{-2l(l+1)(l+2)}{(2l+3)(2l-1)}$	$\frac{l(l+1)}{(2l+3)(2l-1)}$
$l+1$	$l+2$	$\frac{(l+1)(l+2)(l+3)}{(2l+1)(2l+3)}$	$\frac{1(l+1)(l+2)}{(2l+1)(2l+3)}$

$B_3=-\gamma/5$. Similar coefficients are given in Ref. [14].

APPENDIX B

For s subshells, the selection rules limit the outgoing waves to p waves for the dipole term of the matrix element of Eq. (17) and to d waves for the quadrupole term of Eq. (18). As shown previously [2,14] and is apparent from Eq. (26), $\delta=0$ and $\gamma=3\alpha\omega Q_{\omega,2}/R_{\omega,1}\cos(\delta_2-\delta_1)$, or alternatively $B_1=-B_3$. The result can be obtained by considering the angular part of the product of Eqs. (17) and (18), which is

$$D^{(1)}_{\bar{m}0}(\alpha,\beta,\gamma)[D^{(2)}_{M1}(\alpha,\beta,\gamma)-D^{(2)}_{M-1}(\alpha,\beta,\gamma)] . \quad \text{(B1)}$$

For s subshells only $m=0$ terms contribute. The product in Eq. (B1) then reduces to

$$D^{(1)}_{00}(\alpha,\beta,\gamma)[D^{(2)}_{01}(\alpha,\beta,\gamma)-D^{(2)}_{0-1}(\alpha,\beta,\gamma)] = \sqrt{6}\cos^2\beta\sin\beta\cos\alpha , \quad \text{(B2)}$$

where $\beta=\theta$ and $\alpha=\phi$. This result shows that the $m=0$ component of the sum over the values of $m=0,\pm1$ in Eq. (19) only contributes to γ. Nonzero values of δ are due to the $m=\pm1$ components [21].

APPENDIX C

The "velocity" and "acceleration" forms of the radial dipole matrix element for an electron moving in a central potential have been derived previously [16]. The same procedure can be used to obtain alternative forms for the radial matrix elements corresponding to higher multipoles. Consider the radial equations

$$\frac{d^2R_{nl}}{dr^2}+\left[V(r)-\frac{l(l+1)}{r^2}+E_n\right]R_{nl}=0 , \quad \text{(C1)}$$

$$\frac{dR^2_{\bar{n}\bar{l}}}{dr^2}+\left[V(r)-\frac{\bar{l}(\bar{l}+1)}{r^2}+E_{\bar{n}}\right]R_{\bar{n}\bar{l}}=0 , \quad \text{(C2)}$$

for two radial orbitals at different energies. Multiplying each orbital equation by r^p times the other orbital and integrating over r yields

$$\langle R_{nl}r^pR_{\bar{n}\bar{l}}\rangle=\frac{1}{(E_n-E_{\bar{n}})}\times\left[\langle R_{\bar{n}\bar{l}}r^{p-2}R_{nl}\rangle[\bar{l}(\bar{l}+1)-l(l+1)]+\left\langle\frac{d^2R_{nl}}{dr^2}r^pr_{\bar{n}\bar{l}}\right\rangle-\left\langle\frac{d^2R_{\bar{n}\bar{l}}}{dr^2}r^pR_{nl}\right\rangle\right] . \quad \text{(C3)}$$

Integrating by parts, the derivative terms reduce to

$$\left\langle\frac{d^2R_{nl}}{dr^2}r^pR_{\bar{n}\bar{l}}\right\rangle-\left\langle\frac{d^2R_{\bar{n}\bar{l}}}{dr^2}r^pR_{nl}\right\rangle=-\left\langle R_{\bar{n}\bar{l}}\left[p(p-1)r^{p-2}R_{nl}+2pr^{p-1}\frac{dR_{nl}}{dr}\right]\right\rangle . \quad \text{(C4)}$$

For $p=1$ Eq. (C4) reduces to the integral over the product of one radial wave function and the derivative of the other radial wave function and with Eq. (C3) yields the velocity form for the dipole radial matrix element. For $p=2$ the velocity form for the quadrupole matrix element is

$$\langle R_{nl}r^2R_{\bar{n}\bar{l}}\rangle=\frac{1}{(E_n-E_{\bar{n}}}\times\left[\langle R_{\bar{n}\bar{l}}R_{nl}\rangle[l(l+1)-\bar{l}(\bar{l}+1)-2]-4\left\langle r_{\bar{n}\bar{l}}r\frac{dR_{nl}}{dr}\right\rangle\right] . \quad \text{(C5)}$$

Since nl may represent either the initial- or final-state orbital there are two forms of the velocity matrix element. Both were evaluated in the calculations reported here.

[1] J. W. Cooper, Phys. Rev. A **42**, 6942 (1990).
[2] A. Bechler and R. H. Pratt, Phys. Rev. A **39**, 1774 (1989).
[3] A. Bechler and R. H. Pratt, Phys. Rev. A **42**, 6400 (1990).
[4] J. H. Scofield, Phys. Rev. A **40**, 3054 (1989); Phys. Scr. **41**, 59 (1990).
[5] M. O. Krause, Phys. Rev. **177**, 151 (1969).
[6] F. Wuilleumier and M. O. Krause, Phys. Rev. A **10**, 242 (1974).
[7] H. A. Bethe and E. E. Salpeter, *Quantum Mechanics of One- and Two-Electron Systems* (Academic, New York, 1957), p. 248.
[8] J. Cooper and R. N. Zare, J. Chem. Phys. **48**, 942 (1968).
[9] J. C. Tully, R. S. Berry, and B. J. Dalton, Phys. Rev. **176**, 95 (1968).
[10] A. R. Edmonds, *Angular Momentum in Quantum Mechanics* (Princeton University Press, Princeton, NJ, 1957), Chap. 4.
[11] M. Peskin, Adv. Chem. Phys. **18**, 1 (1970).
[12] H. K. Tseng, R. H. Pratt, S. Yu, and A. Ron, Phys. Rev. A **17**, 1061 (1978).
[13] M. S. Wang, Y. S. Kim, R. H. Pratt, and A. Ron, Phys. Rev. A **25**, 857 (1982).
[14] M. Ya Amusia and N. A. Cherepkov, *Case Studies in Atomic Physics* (North-Holland, Amsterdam, 1975), Vol. 5, pp. 154–157.
[15] F. Herman and S. Skillman, *Atomic Structure Calculations* (Prentice-Hall, Englewood Cliffs, NJ 1963).
[16] S. T. Manson, in *Advances in Electronics and Electron Physics,* edited by L. Morton (Academic, New York, 1976), Vol. 41, p. 73.
[17] I. M. Band, Yu. I. Kharitonov, and M. B. Trhaskovskaya, At. Data Nucl. Data Tables **23**, 443 (1979).
[18] D. J. Kennedy and S. T. Manson, Phys. Rev. A **5**, 227 (1972).
[19] A. Ron, R. H. Pratt, and H. K. Tseng, Chem. Phys. Lett. **47**, 377 (1977).
[20] D. W. Lindle, T. A. Ferrett, P. A. Heimann, and D. A. Shirley, Phys. Rev. A **37**, 3808 (1988).
[21] In Ref. [1] it was incorrectly stated that $\delta=0$ for all subshells since only $m=0$ components contribute to the sum. See Errata, Phys. Rev. A **45**, 3362 (1992).